Improving Solar Air Heater Thermal Efficiency Through Computational Fluid Dynamics Analysis

[1]Saurav Kumar Singh, [2]Prof. Pankaj Badgaiyan, [3]Prof. Amit Kumar Asthana

[1]Saurav Kumar Singh, M. Tech Scholar, Department of Energy Technology, Truba Institute of Engineering & Information Technology, Bhopal, MP, India.

[2]Prof. Pankaj Badgaiyan, Assistant Professor, Department of Energy Technology, Truba Institute of Engineering & Information Technology, Bhopal, MP, India.

[3]Prof. Amit Kumar Asthana, Assistant Professor, Department of Energy Technology, Truba Institute of Engineering & Information Technology, Bhopal, MP, India.

Email-: [1]sauravpratapsingh11@gmail.com [2]pankajbadgaiyan33@gmail.com

* Corresponding Author: Saurav Kumar Singh

Abstract: *Innovative tools called solar air heaters (SAHs) are made to capture the sun's heat and use it as a sustainable source of heat for a variety of uses. The use of specialized components to capture and transform solar radiation into thermal energy is highlighted in this overview of the principles of solar energy utilization in SAHs. This study also explores the use of artificial roughness and computational fluid dynamics (CFD) analysis to improve the thermal performance of SAHs in the region of central India. CFD analysis is used to assess the temperature distribution and thermal efficiency of four different SAH configurations, including winglet ribs, V-pattern ribs, broken V-pattern ribs, and multi L-pattern ribs. The results offer useful information for improving SAH designs for improved heat transfer.*

Keywords: *Solar energy, Solar air heater, artificial roughness, CFD analysis, thermal performance, temperature distribution, sustainable heat source.*

I. INTRODUCTION

Solar air heater (SAH) is a device in which energy from sun is captured by absorbing surface and the thermal energy is extracted by the air flowing over it [1]. A solar air heater stands as a remarkable embodiment of renewable energy ingenuity, conceived with the purpose of capturing the sun's radiant energy and transforming it into a practical source of heat. Engineered with precision, these devices excel in harnessing sunlight and converting it into heat energy, which is then channeled into the air for diverse applications. This technology finds its versatile footing across a spectrum of uses, playing a pivotal role in space heating for residences, offices, and factories. Beyond this, solar air heaters seamlessly integrate into ventilation systems, preheating incoming air and alleviating the energy load required to maintain comfortable indoor temperatures. Notably, industrial sectors too benefit from their prowess, as solar air heaters contribute to sustainable heat sources for vital manufacturing processes.

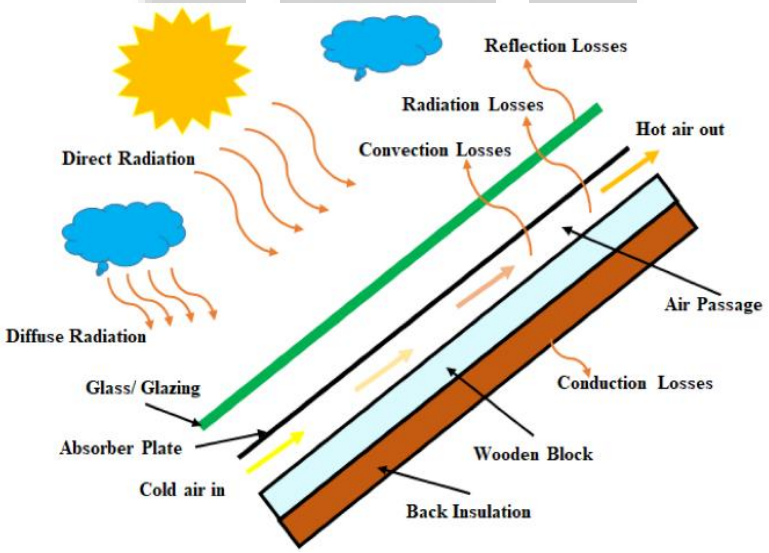

Figure 1. Schematic Presentation of Solar Air Heater

Yet, the brilliance of solar air heaters extends beyond its functional prowess, encapsulating a holistic commitment to sustainable energy practices. At the core of its impact lies an abundant and perpetually available solar energy resource. By

tapping into this natural bounty, solar air heaters epitomize energy sustainability, effectively addressing heating requirements while diminishing reliance on finite conventional fossil fuels.

A. Harnessing Solar Energy for Air Heating: An Overview

The concept of harnessing solar energy for air heating represents a pivotal advancement in renewable energy utilization. This innovative approach capitalizes on the boundless energy emitted by the sun, transforming it into a practical and sustainable source of heat for various applications [2]. Solar energy, a free and readily available resource, serves as the cornerstone of this process, driving the development of systems desi gned to capture, convert, and distribute solar-derived heat.

In essence, the method involves capturing solar radiation through specialized components such as transparent covers, mirrors, or concentrators. These components allow sunlight to penetrate while minimizing heat loss, thereby facilitating the conversion of sunlight into thermal energy . This accumulated heat is then transferred to air, initiating a natural convection process that propels the warmed air towards its designated application.

B. Artificial Roughness and Heat Transfer Augmentation

Artificial roughness and heat transfer augmentation are concepts used in the field of heat transfer and fluid dynamics to enhance the transfer of heat between a solid surface and a fluid (usually a gas or a liquid). These techniques are employed in various engineering applications where efficient heat exchange is crucial, such as in heat exchangers, cooling systems, and thermal management systems [3].

Artificial Roughness

Artificial roughness refers to intentionally introducing irregularities or protrusions on the surface of a heat transfer component, such as a pipe, duct, or heat exchanger wall. Turbulence is caused by these irregularities, which obstruct the fluid's flow [4]. By encouraging mixing between the fluid layers close to the surface and thereby expanding the fluid-solid surface contact area, turbulence improves the convective heat transfer process. More effective heat transfer follows from this.

Ribs, dimples, grooves, and protrusions are just a few examples of the various artificial roughness structures that can be used. The type of roughness to use and its configuration are determined by the fluid's properties, the flow environment, and the desired degree of heat transfer enhancement.

• Ribs: Raised longitudinal or transverse features on a material's surface. They are used to generate turbulence in the boundary layer, which improves mixing and boosts heat transfer [5–9]. In applications like heat exchangers and turbine blades, where heat exchange is essential, ribs are frequently used. The ribs cause the fluid to flow irregularly, causing vortices and swirls that improve heat transfer.

Dimples are tiny depressions or cavities that appear on the surface of a material. In areas where reducing fluid flow resistance is crucial, like aerodynamics and sporting goods like golf balls, dimpling is frequently used to reduce drag. A turbulent boundary layer that is induced by dimples can lessen pressure drag and delay flow separation [10–12]. Improvements in general performance and effectiveness result from this.

These synthetic roughness structures each have particular benefits and uses:

• Ribs: Ribs are frequently used in cooling systems, gas turbine blades, and heat exchangers because they effectively improve heat transfer.

• Dimples: These effective drag-reducers are frequently found in aerodynamics and sporting goods like golf balls and swimwear.

• Grooves: Popular in hydrodynamic and aerodynamic applications, effective at reducing flow separation.

• Protrusions: Protrusions are useful for enhancing heat transfer and are frequently found in heat sinks, exchangers, and electronic cooling.

Heat Transfer Augmentation

Enhancing the rate at which heat is transferred from a hot surface to a cooler fluid is known as heat transfer augmentation. Conduction, convection, and radiation are just a few ways to accomplish this. The emphasis in this article is on forced or natural convection, which is a method of transferring heat from a solid surface to a fluid [13].

Using external devices like fans or pumps, forced convection involves forcing a fluid (liquid or gas) to flow over the surface. By encouraging turbulent flow and raising the heat transfer coefficient, heat transfer enhancement techniques, such as artificial roughness, are used to accelerate heat transfer.

The difference in density brought on by temperature gradients drives fluid motion in natural convection. Techniques for heat transfer augmentation in natural convection situations might involve changing the shape of the heated surface, using fins or extended surfaces, or introducing obstacles that disrupt the natural flow patterns and promote better heat exchange.

II. LITERATURE REVIEW

In the investigation conducted by MSW **Potgieter et. al. [14],** the diverse applications of solar air heaters (SAHs), ranging from space heating to industrial pre-heating and material drying, are outlined. The study centers on evaluating a unique SAH design in terms of thermal efficiency and temperature distribution. This innovative design combines parallel and counter flows to enhance heat transfer and reduce mass. The evaluation employs computational fluid dynamics (CFD) and experimental methods, with computational models validated against experimental data. These models account for solar load, radiation, conduction, convection, and turbulence. Results indicate average conversion efficiency ranging from 23% to 83% and average collector efficiency between 11% and 44%. Although the models over-predict thermal efficiency by 6.75% to 9.01%, they align well with experimental values. Temperatures show qualitative agreement but less quantitative consistency. Despite t his, the study significantly contributes to understanding this novel SAH design's thermal behavior.

In the work by **B Jia et. al. [15],** a novel approach to solar air heaters (SAHs) is introduced, employing a spiral shape of spoilers in place of the conventional serpentine shape. The study investigates the functionality of these spiral solar air heaters (SSAHs), analyzing heat collection efficiency, temperature differentials, irradiance, and air volume. Experimental findings reveal linear temperature differentials concerning irradiation and a quadratic relationship between heat collection efficiency and irradiation with a constant flux. The heat loss coefficient of SSAH is determined as 5.69 W m−2 K−1. SSAHs exhibit higher heat collection efficiency when compared to traditional serpentine SAHs, positioning them as a promising advancement in solar thermal technology.

H Hassan et. al. [16] centers on a newly devised design of solar air heater (SAH) termed the tubular solar heater (TSAH). This innovative design substitutes the flat absorber plate of conventional flat SAHs with adjacent tubes aligned with the airflow direction. Comparative experiments involving both flat SAHs and TSAHs are conducted to assess their performance at varying airflow rates. Results unveil TSAH's superior efficiency, output power, outlet air temperature, and reduced top heat loss compared to flat SAHs. TSAH achieves a significant rise in outlet air temperature, outperforming previous SAH designs, with an average daily efficiency increase of up to 132.6%. TSAH's innovative configuration holds promising potential for advancing the efficiency and effectiveness of solar air heaters.

In the investigation led by **HS Arunkumar et. al. [17],** the application of solar air heaters (SAHs) in both household and industrial settings is highlighted. To address the challenge of reduced thermal efficiency in SAHs, researchers have turned their attention toward enhancing thermal performance through artificial flow modification techniques. This approach disrupts the laminar sub-layer beneath the absorber plate, elevating air turbulence levels and subsequently boosting heat transfer rates. The study delves into the influence of diverse turbulator shapes employed by different researchers to enhance air heater performance. It thoroughly explores design considerations, geometries, flow conditions, and their effects on turbulence, heat transfer rates, absorber temperatures, and thermo-hydraulic enhancement factors. Concluding remarks suggest potential directions for further improvements in solar air heater performance.

In the work by **A Saxena et. al. [18],** the context of numerous solar energy applications for cooking, heating, cooling, and power generation is acknowledged. Among these applications, solar air heaters (SAHs) play a significant role, specifically in drying, timber seasoning, and space heating. The study details the design of a SAH aimed at achieving elevated exhaust temperatures, even during adverse ambient conditions or off-peak solar hours. A unique blend of desert and granular carbon is employed as thermal heat storage within the SAH. By integrating halogen lights within the inlet and outlet ducts, exhaust temperature is further enhanced. Natural and forced convection experiments are conducted to evaluate the performance of two similar SAH designs—one with heat storage and one without. The study's outcomes reveal thermal efficiencies ranging from 18.04% to 20.78% under natural convection and 52.21%–80.05% with forced convection.

C Mahboub et. al. [19] underscores the pivotal role of suitable design in ensuring cost-effective solar air heaters. While various techniques have been proposed to enhance SAH performance through turbulence promoters, achieving a balance between cost and effectiveness remains a challenge. The study introduces an optimized solar air heater design, featuring a slightly curved smooth flow channel with a convex-shaped absorber plate. A prototype is constructed and tested, showcasing improved overall efficiency compared to conventional flat plate heaters under similar operating conditions.

In the study by **V Goel et. al. [20],** the widespread utilization of solar air heaters (SAHs) for efficient solar radiation collection and utilization is acknowledged. The article's focus lies in offering a comprehensive literature review spanning history, fundamentals, and recent advancements within the field of solar thermal air heating systems. Various collector designs, including evacuated tubes, flat plates, and multiple passages, are explored and discussed. Techniques for performance enhancement, such as artificial roughness, fins, baffles, and vortex generators, are analyzed and compared through thermohydraulic performance assessments, aiming to identify optimal configurations for practical applications.

III. OBJECTIVES

The present work is driven by the following objectives.

1. The primary goal of this study is to conduct a CFD analysis on the base model in order to elevate the thermal performance of a solar air heater tailored for the central India region.

2. Varied CAD models of the solar air heater will be developed by adjusting the roughness width, with the aim of optimizing thermal performance.
3. A computational fluid dynamics analysis will be carried out on the proposed solar air heater designs, enhancing our understanding of their fluid dynamics and heat transfer characteristics.
4. By comparing the results across all the solar air heater designs, the objective is to identify the most effective configuration and provide recommendations for optimal performance.

V. METHODOLOGY

The solar air heater comprises an absorber plate positioned atop a parallel plate, forming a narrow passage through which air is directed for heating. A transparent cover system is situated above the absorber plate. The lower and lateral sections are enclosed by a sheet metal container filled with insulation. The entire assembly is enclosed in a box made of sheet metal that is angled appropriately. The execution of mathematical and computational fluid dynamics (CFD) analyses for the solar air heater is the focus of this chapter.

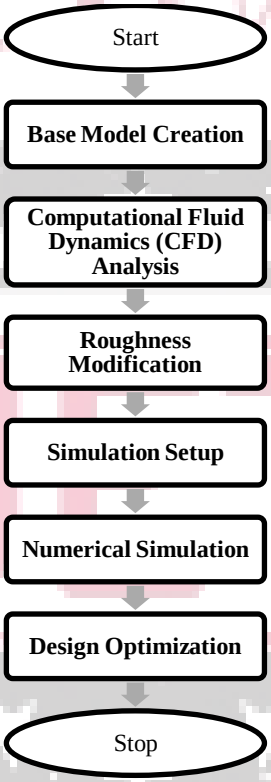

Figure 2. Flowchart for Proposed Methodology

In order to comprehend fluid flow and heat transfer, the methodology involves developing a base model with CAD software, then analyzing the results with Computational Fluid Dynamics (CFD). By altering the absorber plate's roughness, different CAD models are produced to enhance heat transfer. Simulation setups define conditions, and numerical simulations yield temperature distributions and heat transfer rates. Boundary conditions, including air temperature and solar radiation, are considered. The impact of roughness modifications on thermal performance is analyzed, leading to the identification of an optimal design configuration for solar air heater applications in central India.

A. Analyzing Solar Air Heater Using Mathematical Equations

Energy flow within a solar air heater involves the absorption of solar radiation by the absorber plate, which heats up. The heated plate then transfers thermal energy to the passing air through convection, raising its temperature. As the heated air exits the collector, it carries away the absorbed heat. Meanwhile, losses occur through conduction to the surroundings and radiation from the collector's surface. The net result is an increase in the air's temperature, making it suitable for various heating applications.

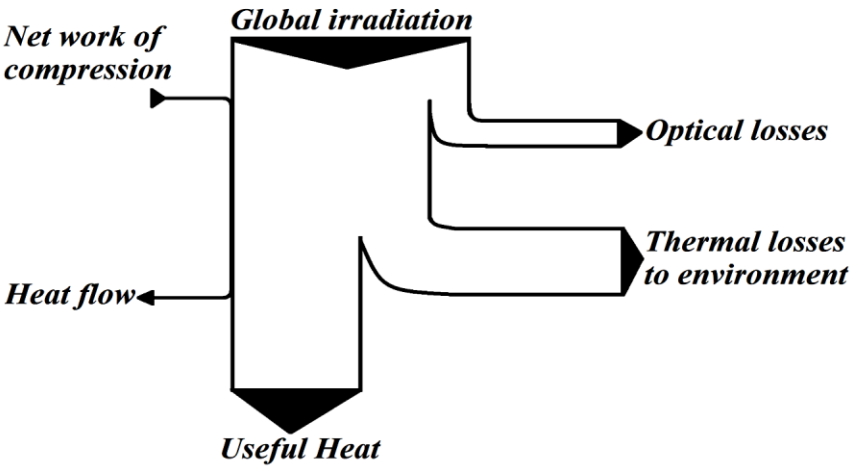

Figure 3. Circulation of Energy in Solar Based Air Heater

Upon reviewing the energy flow diagram of the solar air heater, it becomes evident that the beneficial heat gain is achieved through the subtraction of optical losses and thermal losses to the environment, as illustrated.

Several assumptions have been taken into account in the analysis: Firstly, as the air traverses a distance dx, the bulk mean temperature changes from Tf to (Tf+dTf). Secondly, the air mass flow rate is denoted as ṁ. Thirdly, any variations in the mean temperatures of both the absorber plate (Tpm) and the plate below (Tbm) are considered negligible for simplification. Lastly, side losses are disregarded due to their minimal impact on the overall analysis.

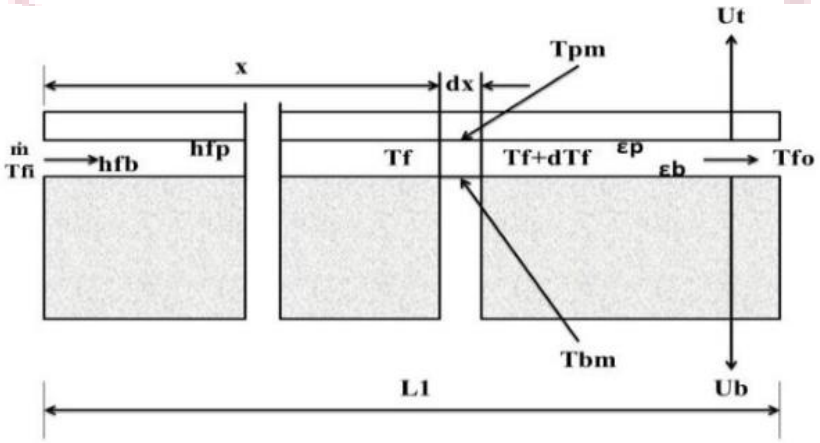

Figure 4. Assessment of traditional solar air heater

For Absorber Plate

$$SL_2.dx = U_t.(L_2 dx T_{pm} - L_2 dx T_{pa}) + (h_{fb} L_2 dx T_{pm} - h_{fb} L_2 dx T_f) + \frac{\sigma L_2}{\frac{\varepsilon_b + \varepsilon_p}{\varepsilon_p \varepsilon_b} - 1} dx\left((T_{pm})^{2^2} - (T_{bm})^{2^2}\right)$$

For bottom plate

$$\frac{\sigma L_2}{\frac{\varepsilon_b + \varepsilon_p}{\varepsilon_p \varepsilon_b} - 1} dx\left((T_{pm})^{2^2} - (T_{bm})^{2^2}\right) = h_{fb} L_2 dx T_{pm} - h_{fb} L_2 dx T_f + U_b.(L_2 dx T_{bm} - L_2 dx T_{bm})$$

For air stream

$$mc_p dT_f = (h_{fb} L_2 dx T_{pm} - h_{fb} L_2 dx T_f) + (h_{fb} L_2 dx T_{bm} - h_{fb} L_2 dx T_f)$$

Where

S = flux absorbed in the absorber plate

U_t and U_b = top loss and bottom loss coefficient based on the temperature difference $(T_{pm} - T_a)$, $(T_{bm} - T_a)$

h_{fp} and h_{fb}= convective heat transfer coefficient between the absorber plate and air stream; and bottom plate and air stream

ε_p ε_b= emissivity of the absorber plate and bottom plate surface

Table 1 Showcases the dimensional and thermal parameters pertaining to the suggested solar air heater, as documented by A. Kumar in 2021

Parameter	Value/Range	Parameter	Value/Range	Parameter	Value/Range
Collector Dimensions		**Thermal Conductivity**		**Insulation Thickness**	
Length (L)	1.24 m	Insulation (kins)	0.037 W/mK	Base (tb)	0.05 m
Width (W)	0.16 m	Glass (kg)	0.75 W/mK	Side (ts)	0.05 m
Duct Depth (Dd)	0.04 m	**Radiative Properties**		**Surface Roughness**	
Angles and Temperatures		Transmissivity-absorptivity product (τα)	0.88	Roughness Height (e)	3 mm
Angle of Attack (α)	30°-75°	Absorber Plate Emissivity (ϵp)	0.9	Relative Roughness Pitch (P/e)	0.5-12
Ambient Temperature (Ta)	300 K	Glass Cover Emissivity (ϵg)	0.88	Relative Roughness Width (W/w)	0.3-7
Inlet Temperature (Ti)	300 K	**Glass Cover**			
Sun Temperature (Tsun)	5778 K	Thickness (tg)	0.004 m		
Air Velocity		Air Gap (Lgp)	0.005 m		
Atmospheric Wind Velocity (Vwind)	1 m/s	**Collector Edge**			
Flowing Air Velocity (V)	1.12-5.23 m/s	Thickness (te)	0.04 m		

Solar load calculation

Solar load estimation for the chosen position at Latitude 23° 17' N and Longitude 77° 27' 21" E has been employed.

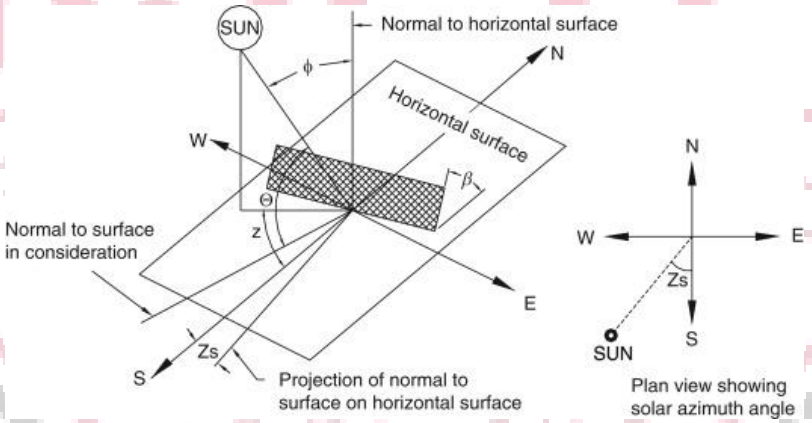

Figure 5. Solar angles diagram

Latitude Angle (∅): The angle formed by a radial line that connects the specified location to the Earth's center. In this context, the latitude angle measures 23.283 degrees and is projected onto the equator plane.

Hourly Global, Diffuse and beam radiations on horizontal surface under cloudless skies

The hourly global radiation I_g on a horizontal surface is the sum of the hourly beam radiation, I_b and the hourly diffuse radiation I_d

$$I_g - I_b = I_d$$

If the I_{bn} is the beam radiation on the surface normal to the direction of the sun rays, the beam radiation received on a horizontal surface may be given as

$$I_b = I_{bn} \cos \theta_z$$

$$I_g - I_d / I_{bn} = \cos \theta_z$$

I_{bn} and I_d are estimated as

$$I_{bn} = A \exp(-B/\cos\theta_z)$$

$$\frac{I_d}{I_{bn}} = C$$

Where A, B & C are constant whose value have been determined month wise on the basis of measurements.

The months range from January to December, with corresponding values for parameters A, B, and C. These parameters are used in a formula to estimate the hourly solar irradiance. A represents the solar radiation intensity in watts per square meter (W/m²), B is a coefficient, and C is another coefficient. Each month has specific values for these parameters, which are crucial for accurate solar radiation predictions. For instance, during the first month, A is 1205 W/m², B is 0.139, and C is 0.102. Similarly, the values for the remaining months are provided in the table.

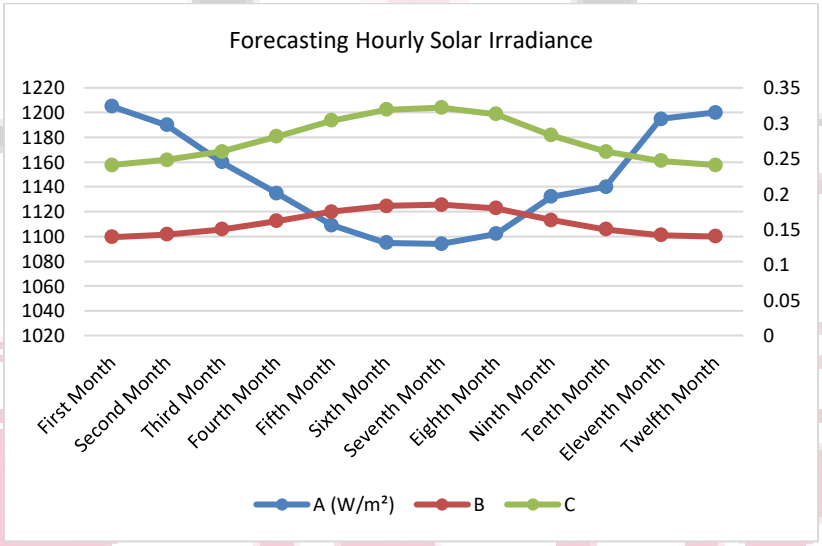

Figure 6. Forecasting Hourly Solar Irradiance

Validation of the work

To validate the current study, the dimensional parameters of the solar air heater were sourced from a research paper authored by Amit Kumar and Apurba Layek in 2021 titled "Energetic and Exergetic Based Performance Evaluation of Solar Air Heater Having Winglet Type Roughness on Absorber Surface," published in Solar Energy Materials & Solar Cells (Volume 230, 2021, Article 111147). The paper's DOI is *10.1016/j.solmat.2021.111147*.

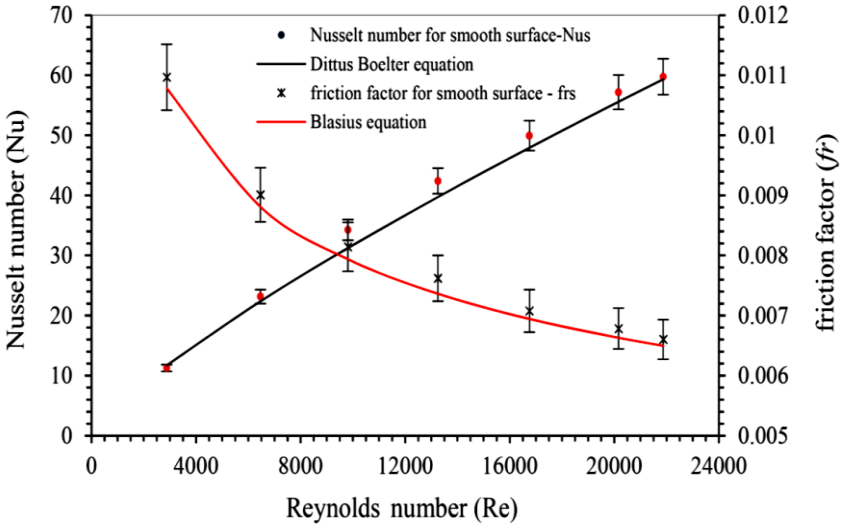

Figure 7. Variation of Nusselt Number and Friction Factor with Different Reynolds Numbers according.

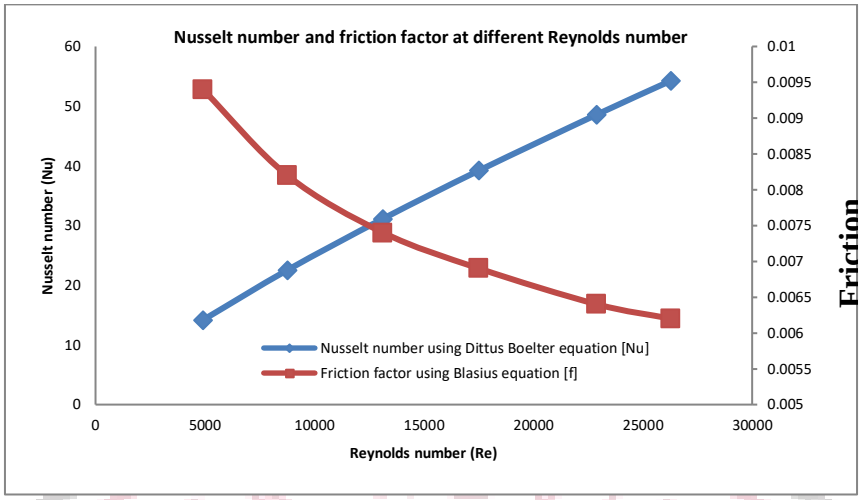

Figure 8. Variation of Nusselt Number and Friction Factor with Different Reynolds Numbers in the Present Study

Upon comparing the results from both the reference paper and the present study under the same parameters, a distinct trend emerges: with an increase in Reynolds number, the Nusselt number rises while the friction factor decreases. This observation aligns with the findings presented.

V. RESULT AND DISCUSSION

The primary aim of this study is to employ computational fluid dynamics (CFD) analysis in order to predict the thermal efficiency of a solar air heater specific to the Bhopal location. To achieve this goal, four distinct models of solar air heaters have been constructed: those with winglet ribs, V-pattern ribs, broken V-pattern ribs, and multi L-pattern ribs. Utilizing ANSYS Fluent, a steady-state CFD analysis was conducted for the designated location, characterized by a latitude of 23° 17' 00" N and a longitude of 77° 27' 21" E. The objective was to ascertain the maximum temperature distribution within the solar air heater by initiating an air inlet temperature of 300 K, in tandem with the calculated solar radiations pertinent to the chosen location. This chapter delves into the comprehensive discussion of diverse results emerging from both computational fluid dynamics and mathematical calculations, manifested through contours, graphs, and tables.

A. Findings and Discussion for Mathematical Analysis

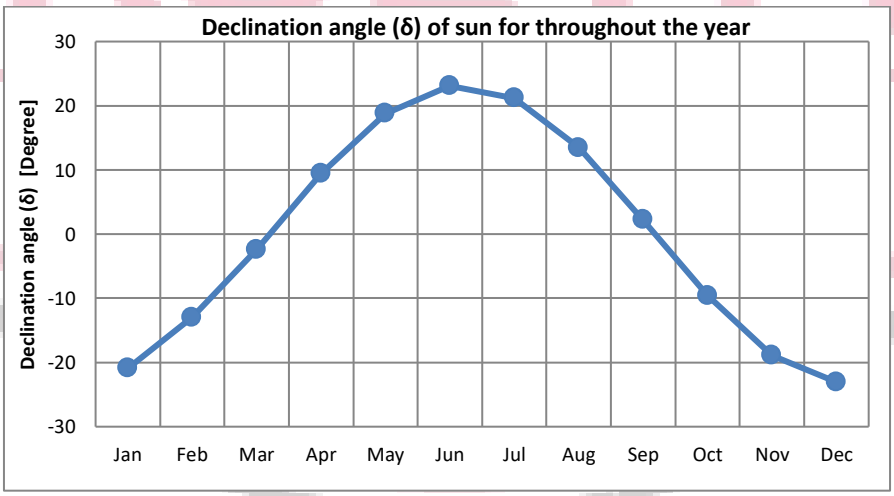

Figure 9. Declination angle (δ) of sun for throughout the year

The graph 5.1 displays variations in declination angles across the months. It is evident that the maximum declination angle occurs in June, reaching 23.08591, while the minimum is observed in December, dipping to -23.0496. These shifts in declination angles signify the changing solar angle with respect to the Earth's equatorial plane throughout the year. Such variations play a significant role in influencing solar radiation and energy distribution, ultimately impacting the performance of solar energy systems like air heaters.

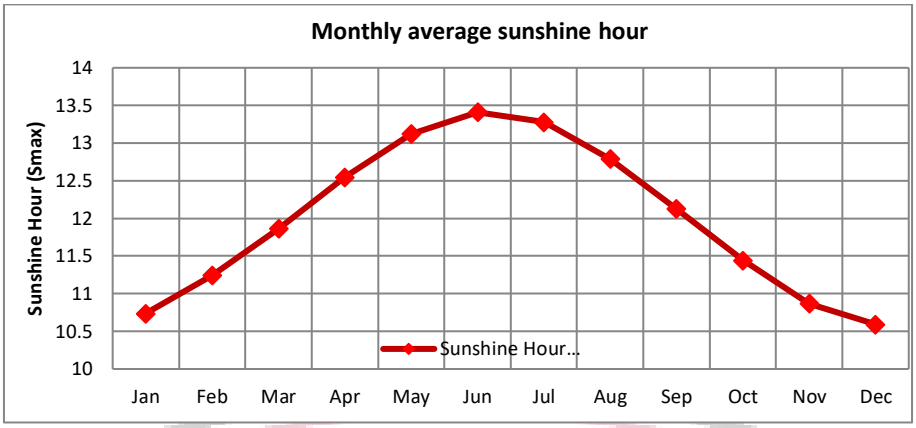

Figure 10. Monthly average sunshine hour

The highest monthly average sunshine hour is 13.40921 hours in the month of June, while the lowest is 10.59329 hours in December. This fluctuation in sunshine hours over the months reflects the changing solar exposure and daylight duration throughout the year. These variations are crucial for assessing the potential solar energy generation and utilization in various applications, including solar air heaters.

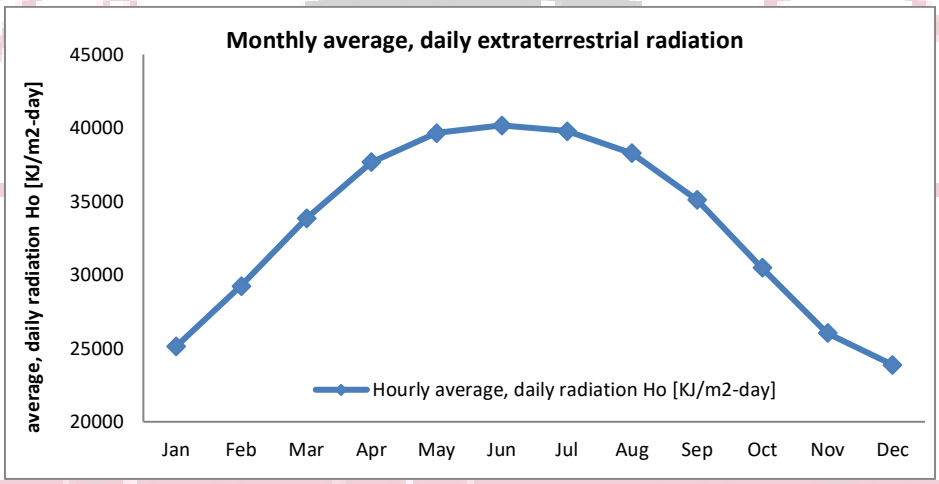

Figure 11. Monthly average, daily extraterrestrial radiation that would fall on horizontal surface in the absence of atmosphere

The peak value for monthly average, daily extraterrestrial radiation is observed in June, amounting to 40173.09 KJ/m²-day, while the lowest value occurs in December at 23886.74 KJ/m²-day. This variation signifies the changing intensity of solar radiation reaching the Earth's atmosphere throughout the year, influenced by the Earth's orbit and tilt. These fluctuations play a pivotal role in determining the solar energy availability and its potential utilization for various applications, including solar air heaters.

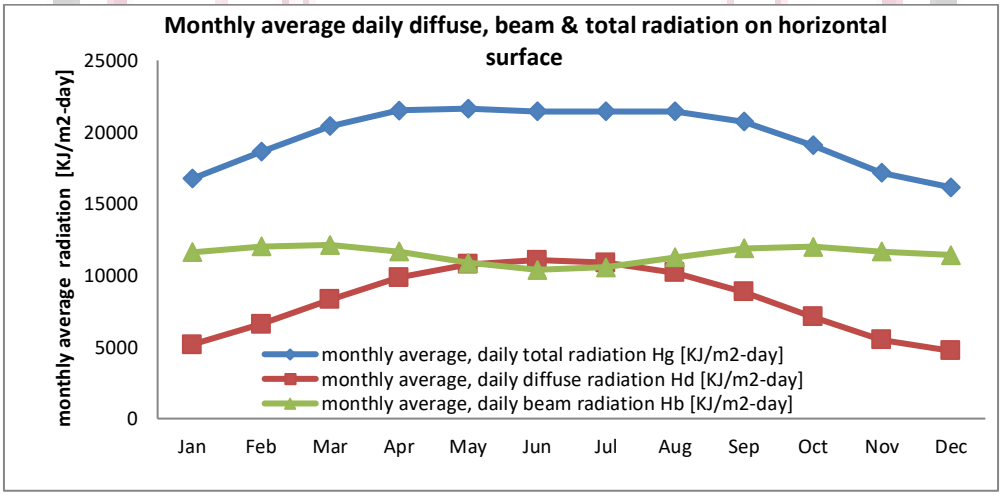

Figure 12. Monthly average daily diffuse, beam & total radiation on horizontal surface

The graph 5.4 presents the monthly average daily diffuse, beam, and total radiation on a horizontal surface. Notably, the highest levels of diffuse radiation are recorded in June, with a peak value of 11062.57 KJ/m²-day. Conversely, the lowest diffuse radiation is observed in December at 4729.266 KJ/m²-day. The monthly average beam radiation reaches its zenith in June, reaching 21448.48 KJ/m²-day, while it reaches its nadir in December with a value of 16143.23 KJ/m²-day. Additionally, the highest total radiation on a horizontal surface occurs in June, totaling 40173.09 KJ/m²-day, whereas the lowest value is seen in December at 23886.74 KJ/m²-day. These variations in radiation levels throughout the months reflect the changing solar exposure, atmospheric conditions, and Earth's tilt angle, all of which significantly influence the performance of solar energy systems like air heaters.

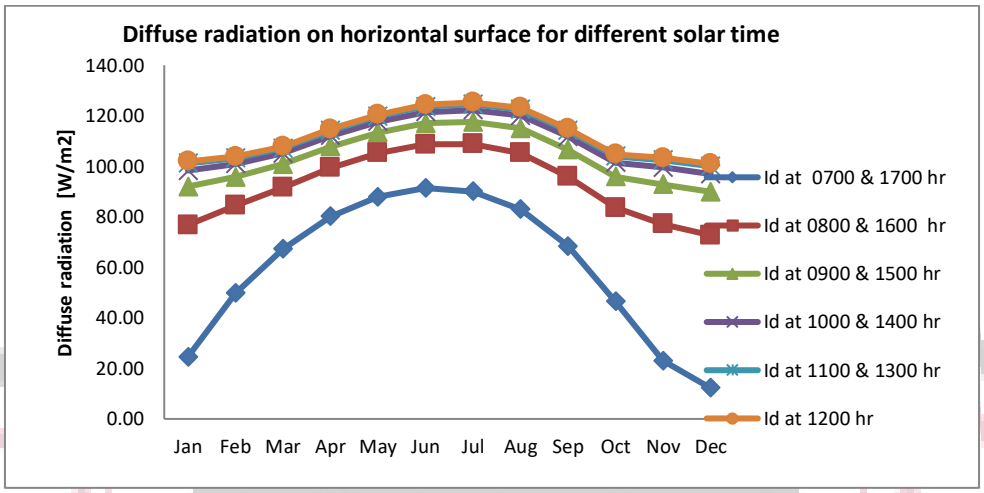

Figure 13. Horizontal Surface Beam Radiation for Various Solar Times

This pattern is consistent for other months as well, with the values generally increasing from sunrise to midday and then decreasing afterward. The amount of diffuse radiation is influenced by factors such as the position of the sun, atmospheric conditions, and the time of year. This information is crucial for understanding the availability of solar energy and designing solar energy systems that take into account variations in radiation throughout the day and across different months.

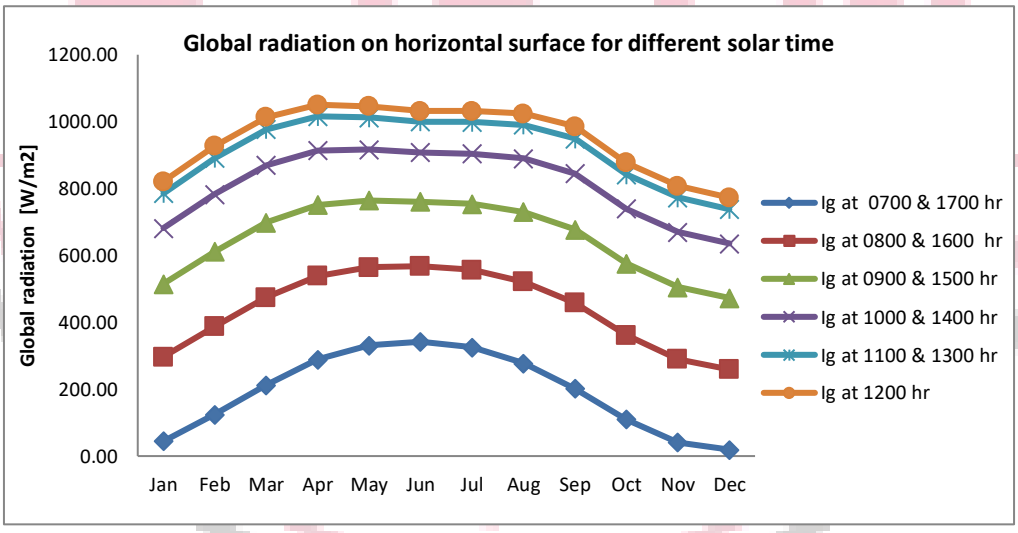

Figure 14. Global solar radiation on a horizontal surface at various solar times

Estimations of direct beam, diffuse, and overall global solar radiations on a horizontal surface under clear sky conditions have been computed through equations 8, 9, 10, and 11, aided by information from Table-5.2 spanning the entire year. The incident beam radiation has been derived for the solar period between 0700 hours and 1700 hours, as illustrated in Figure-5.4. The scattered diffuse radiation due to atmospheric molecules and particles has been assessed and visualized in Figure-5.5, while the cumulative global radiation, representing the combined impact of incident and diffuse radiation, is depicted in Figure-5.6.

B. CFD Investigation of Solar Air Heater

CFD Investigation of Solar Air Heater with Winglet Ribs Configuration:

Upon conducting a computational fluid dynamics analysis on a solar air heater equipped with winglet ribs at an airflow rate of 5.23 m/s, the investigation revealed a notable temperature distribution pattern. Notably, the highest temperature

recorded is 339.2K which is also 65.75°C, achieved at the lower edge of the winglet ribs on the textured surface of the absorber plate within the solar air heater. This observation is visually presented in the accompanying.

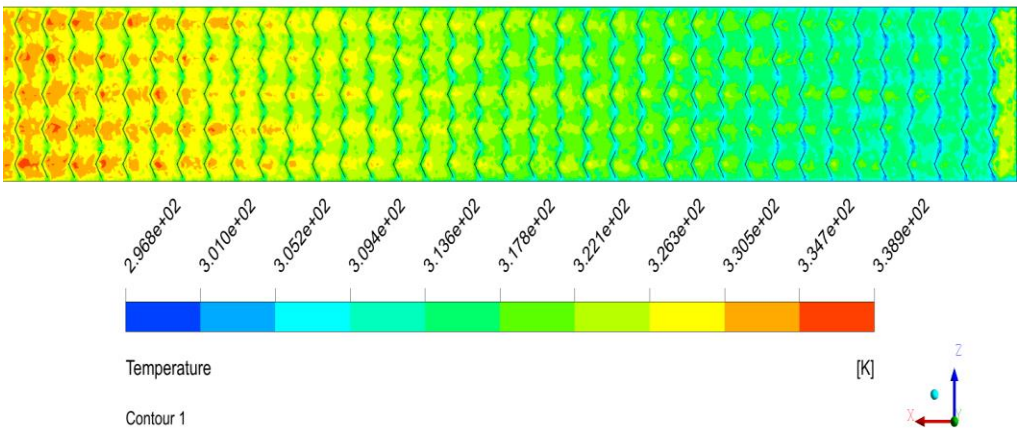

Figure 15. Spatial Variation of Temperature across Solar Air Heater with Winglet Ribs

Exploration of Solar Air Heater with V-Pattern Ribs through Computational Fluid Dynamics Analysis:

Following a computational fluid dynamics analysis on a solar air heater featuring V-pattern ribs, conducted at an airflow rate of 5.23 m/s to investigate temperature distribution, it has been observed that the highest temperature reaches 340.4 K (67.25°C). This peak temperature is achieved at the lower edge of the rough surface of the absorber plate within the solar air heater, as illustrated in the accompanying.

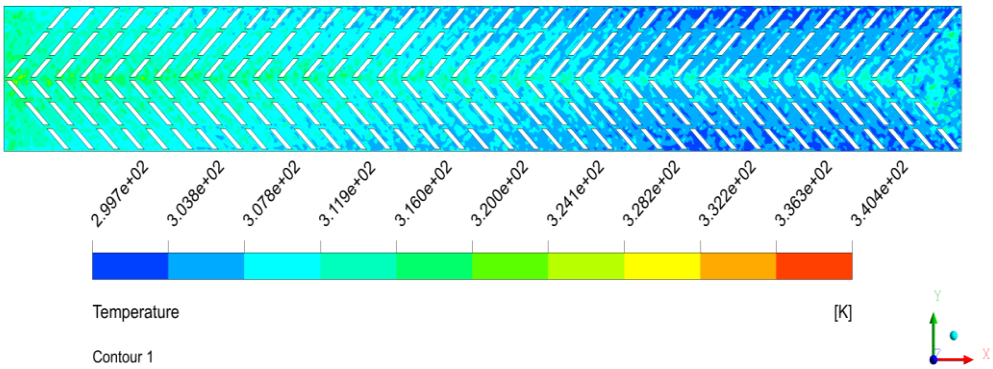

Figure 16. Distribution of Temperatures Across Solar Air Heater with V-Pattern Ribs

Exploration of Solar Air Heater with Broken V-Pattern Ribs through Computational Fluid Dynamics Analysis:

Upon conducting a computational fluid dynamics analysis on a solar air heater featuring broken V-pattern ribs, at an airflow rate of 5.23 m/s to investigate temperature distribution, it has been noted that the highest temperature recorded is 342.0 K (68.85°C). This peak temperature is achieved at the lower edge of the rough surface of the absorber plate within the solar air heater, as visually depicted in the accompanying.

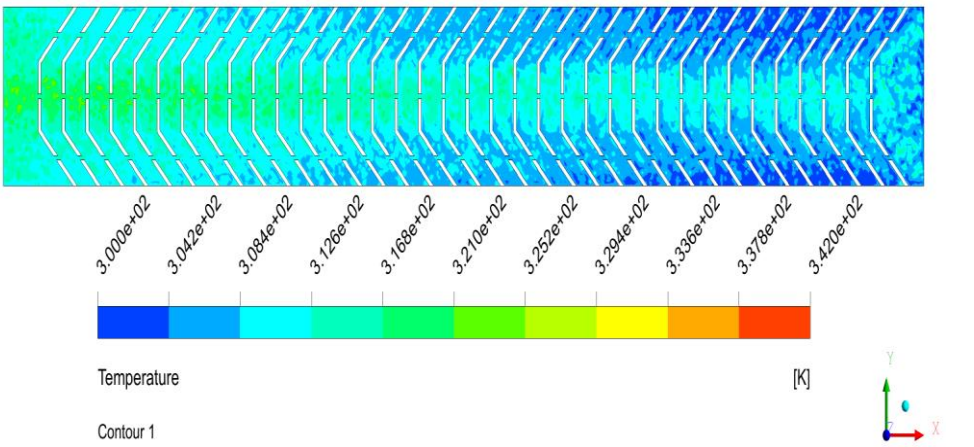

Figure 17. Spatial Variation of Temperature across Solar Air Heater with Broken V-Pattern Ribs

Exploration of Solar Air Heater with Multi L-Pattern Ribs Using Computational Fluid Dynamics Analysis:

Upon conducting a computational fluid dynamics analysis on a solar air heater incorporating multi L-pattern ribs, with an airflow rate of 5.23 m/s to investigate temperature distribution, it has been discovered that the highest temperature reached is 344.6 K (71.45°C). This peak temperature is achieved at the lower edge of the rough surface of the absorber plate within the solar air heater, as illustrated in the accompanying.

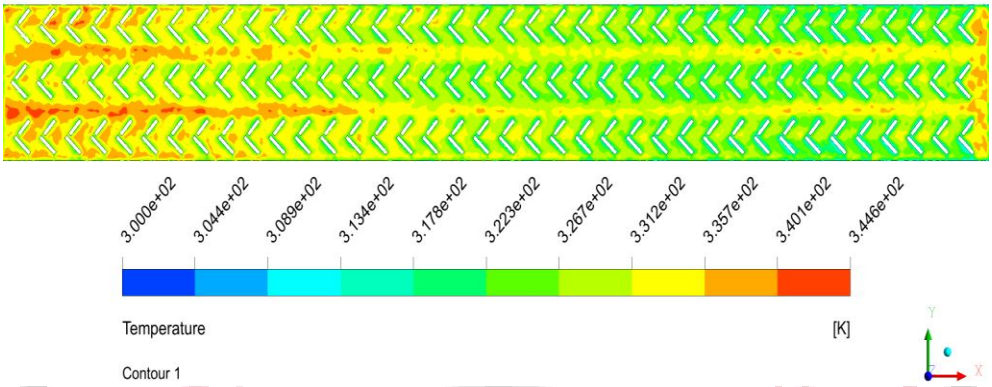

Figure 18. Spatial Variation of Temperature across Solar Air Heater with Multi L-Pattern Ribs

Comparative results of different designs of solar air heater

$$T_{av} = \frac{T_{max}}{2} - \frac{T_{in}}{2}$$

Table 2. Comparative Outcomes Across Various Solar Air Heater Designs

Solar Air Heater Type	Inlet Temperature (°C)	Average Temperature (°C)	Maximum Temperature (°C)
Winglet Ribs	26.85	46.35	65.75
V-Pattern Ribs	26.85	47.05	67.25
Broken V-Pattern Ribs	26.85	47.85	68.85
Multi L-Pattern Ribs	26.85	49.15	71.45

The table 5.5 presents a comparison of various solar air heater designs based on temperature performance. Each design type is assessed for inlet temperature, average temperature, and maximum temperature. The results show that the multi L-pattern ribs design attains the highest maximum temperature of approximately 344.6°C, followed by the broken V-pattern ribs, V-pattern ribs, and winglet ribs designs.

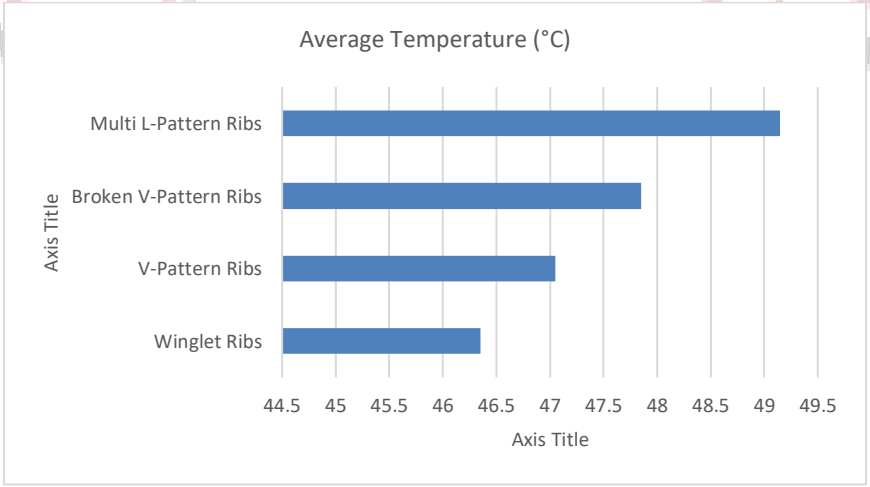

Figure 19. Comparing Average Temperature Results Across Various Solar Air Heater Designs

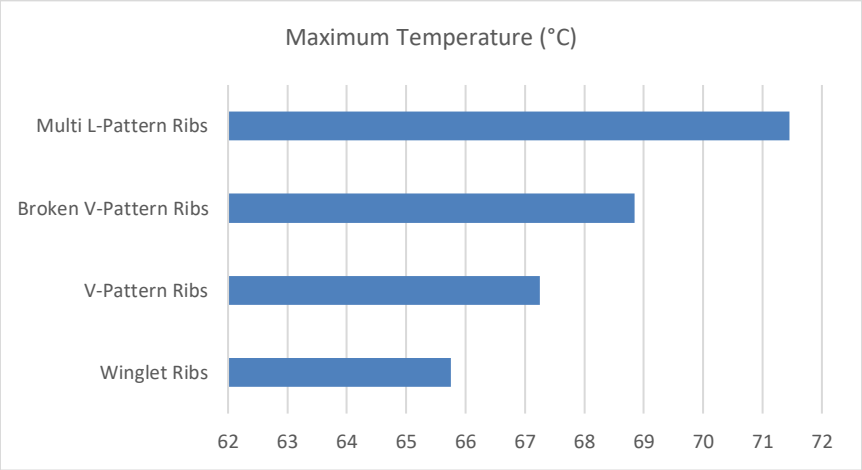

Figure 20. Comparing Maximum Temperature Results Across Various Solar Air Heater Designs

Table 3. Variation in Radiative Heat Transfer Coefficient Among Diverse Solar Air Heater Designs

Solar Air Heater Type	Radiative Heat Transfer Coefficient [W/(m²·K)]
Winglet Ribs	592.702
V-Pattern Ribs	596.429
Broken V-Pattern Ribs	601.008
Multi L-Pattern Ribs	608.178

Table 4. Average wind speed for last five year in the central India

Month						
Months	**2017**	**2018**	**2019**	**2020**	**2021**	**Average wind speed**
Jan	8.6	6.8	9.4	10.8	9.9	**9.10**
Feb	9.4	7.5	10.9	11.1	8.7	**9.52**
Mar	9.9	10.1	12.4	12.1	11.8	**11.26**
Apr	14.3	12.0	13.8	13.0	12.1	**13.04**
May	12.4	14.3	16.3	16.3	15.6	**14.98**
Jun	13.0	16.3	16.9	15.2	17.3	**15.74**
Jul	16.5	17.1	17.7	13.8	16.5	**16.32**
Aug	13.4	16.5	18.2	19.2	15.1	**16.48**
Sep	9.3	12.8	13.9	9.4	11.9	**11.46**
Oct	7.4	7.0	8.0	9.0	7.4	**7.76**
Nov	6.3	6.3	6.7	4.4	9.6	**6.66**
Dec	8.7	8.3	9.8	8.4	9.4	**8.92**

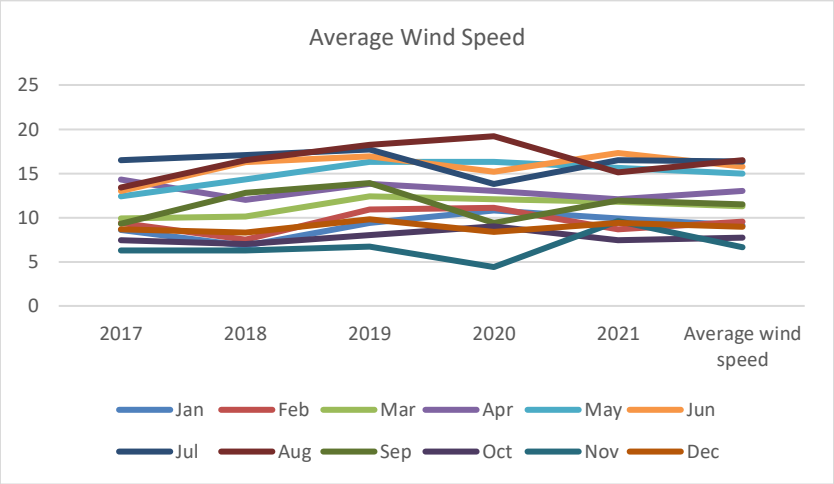

Figure 21. Average wind speed for last five year in the central India

Table 5. Variation in 'e' Values Among Different Solar Air Heater Designs

solar air heater type	$e = 0.430(1 - 100/T_{pm})$
Winglet Ribs	0.2956
V-Pattern Ribs	0.2959
Broken V-Pattern Ribs	0.2961
Multi L-Pattern Ribs	0.2967

Table 6. Total Heat Loss Variation Among Different Solar Air Heater Designs

Solar Air Heater Type	$U_T\ [w/m^2\_k]$	$U_B\ [w/m^2\_k]$	$U_{side}\ [w/m^2\_k]$	$U_L\ [w/m_k^2]$
Winglet Ribs	5.653	0.738	0.208	6.601
V-Pattern Ribs	5.616	0.738	0.208	6.564
Broken V-Pattern Ribs	5.593	0.738	0.208	6.541
Multi L-Pattern Ribs	5.573	0.738	0.208	6.521

Table 7. Variation in Useful Heat Gain Among Different Solar Air Heater Designs

solar air heater type	**Useful heat gain [watt]**
Winglet Ribs	3.624
V-Pattern Ribs	3.560
Broken V-Pattern Ribs	3.493
Multi L-Pattern Ribs	3.382

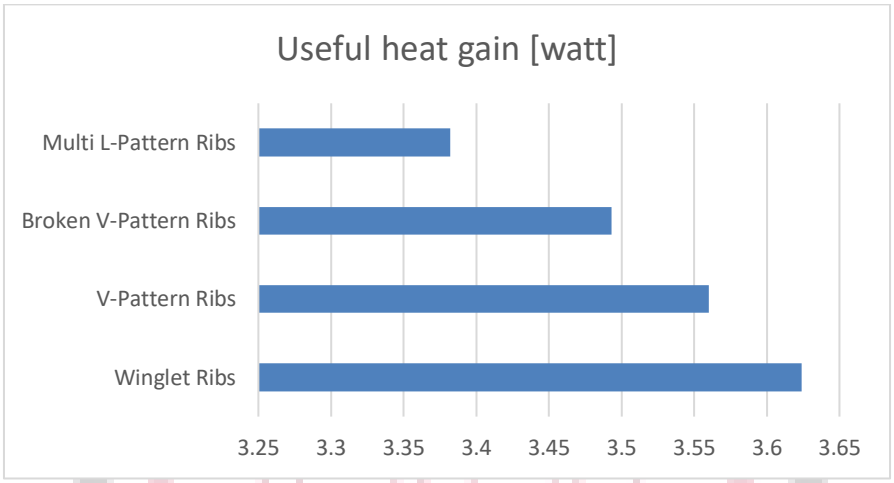

Figure 22. Comparison of Useful Heat Gain Across Various Solar Air Heater Designs

Table 8. Efficiency of Collector, Heat Removal Factor, and Collector Thermal Efficiency Across Various Solar Air Heater Designs

solar air heater type	Collector efficiency factor F'	heat removal factor F_r	Thermal efficiency of collector using heat removal factor
Winglet Ribs	0.4507	0.450	0.3346
V-Pattern Ribs	0.4500	0.449	0.3320
Broken V-Pattern Ribs	0.4491	0.448	0.3290
Multi L-Pattern Ribs	0.4477	0.447	0.3244

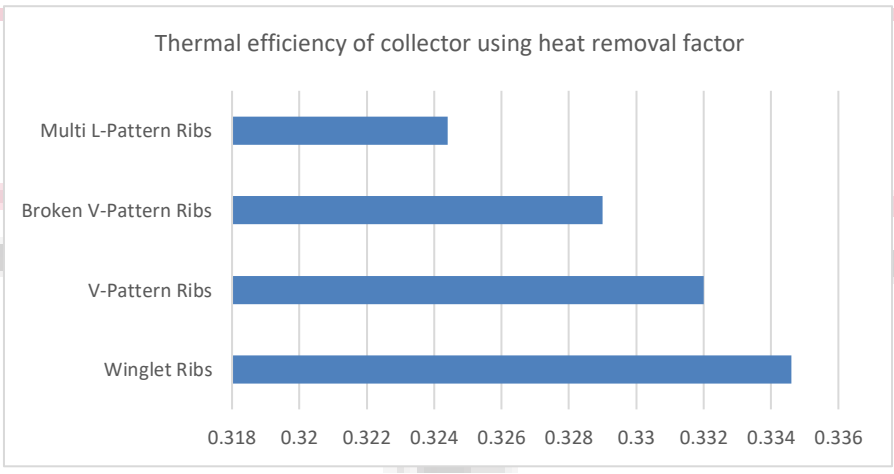

Figure 23. Comparison of Collector Thermal Efficiency Using Heat Removal Factor Across Various Solar Air Heater Designs

VI. CONCLUSION

Emphasizes the significant advancements made in the field of solar air heaters (SAHs) and their potential impact on renewable energy utilization. It highlights the crucial role of specialized components in capturing and converting solar energy into practical heat. Additionally, it underlines the promising results obtained through the application of artificial roughness and computational fluid dynamics (CFD) analysis, specifically tailored for the central India region. The study's findings not only provide valuable data for optimizing SAH designs but also underscore the importance of sustainable energy sources in residential, commercial, and industrial applications. Overall, the conclusion reinforces the positive prospects of clean and renewable energy solutions in our pursuit of a more sustainable future.

REFERENCES

[1] Ahmad, A., Prakash, O., Kumar, A., & Pandey, A. (2020). A Review of Solar Air Heater. Low Carbon Energy Supply Technologies and Systems, 1-10.

[2] Yadav, A. S., & Thapak, M. K. (2014). Artificially roughened solar air heater: Experimental investigations. Renewable and Sustainable Energy Reviews, 36, 370-411.

[3] Bhushan, B., & Singh, R. (2010). A review on methodology of artificial roughness used in duct of solar air heaters. Energy, 35(1), 202-212.

[4] Hans, V. S., Saini, R. P., & Saini, J. S. (2009). Performance of artificially roughened solar air heaters—A review. Renewable and Sustainable Energy Reviews, 13(8), 1854-1869.

[5] Kabeel, A. E., Hamed, M. H., Omara, Z. M., & Kandeal, A. W. (2017). Solar air heaters: Design configurations, improvement methods and applications–A detailed review. Renewable and Sustainable Energy Reviews, 70, 1189-1206.

[6] Goel, V., Hans, V. S., Singh, S., Kumar, R., Pathak, S. K., Singla, M., ... & Saini, R. P. (2021). A comprehensive study on the progressive development and applications of solar air heaters. Solar Energy, 229, 112-147.

[7] Kumar, A., & Subhash, K. (2017). Effect of roughness and glass cover on solar air heater performance-A review. Int. Res. J. of Advanced Engineering and Science, 02,(4), 46, 58.

[8] Jain, S. K., Agrawal, G. D., & Misra, R. (2019). A detailed review on various V-shaped ribs roughened solar air heater. Heat and Mass Transfer, 55, 3369-3412.

[9] Rajarajeswari, K., & Sreekumar, A. (2016). Matrix solar air heaters–A review. Renewable and Sustainable Energy Reviews, 57, 704-712.

[10] Olivkar, P. R., Katekar, V. P., Deshmukh, S. S., & Palatkar, S. V. (2022). Effect of sensible heat storage materials on the thermal performance of solar air heaters: State-of-the-art review. Renewable and Sustainable Energy Reviews, 157, 112085.

[11] Tyagi, V. V., Panwar, N. L., Rahim, N. A., & Kothari, R. (2012). Review on solar air heating system with and without thermal energy storage system. Renewable and Sustainable Energy Reviews, 16(4), 2289-2303.

[12] Jain, P. K., Lanjewar, A., Rana, K. B., & Meena, M. L. (2021). Effect of fabricated V-rib roughness experimentally investigated in a rectangular channel of solar air heater: a comprehensive review. Environmental Science and Pollution Research, 28, 4019-4055.

[13] Ifrim, V. C., & Pop, T. (2022, May). Review of thermal performance enhancement of Solar Air Heater using shapes on absorber plate. In 2022 International Conference on Development and Application Systems (DAS) (pp. 19-27). IEEE.

[14] Potgieter, M. S. W., Bester, C. R., & Bhamjee, M. (2020). Experimental and CFD investigation of a hybrid solar air heater. Solar Energy, 195, 413-428.

[15] Jia, B., Liu, F., & Wang, D. (2019). Experimental study on the performance of spiral solar air heater. Solar Energy, 182, 16-21.+

[16] Hassan, H., Abo-Elfadl, S., & El-Dosoky, M. F. (2020). An experimental investigation of the performance of new design of solar air heater (tubular). Renewable Energy, 151, 1055-1066.

[17] Arunkumar, H. S., Karanth, K. V., & Kumar, S. (2020). Review on the design modifications of a solar air heater for improvement in the thermal performance. Sustainable Energy Technologies and Assessments, 39, 100685.

[18] Saxena, A., Srivastava, G., & Tirth, V. (2015). Design and thermal performance evaluation of a novel solar air heater. Renewable Energy, 77, 501-511.

[19] Mahboub, C., Moummi, N., Brima, A., & Moummi, A. (2016). Experimental study of new solar air heater design. International journal of green energy, 13(5), 521-529.

[20] Goel, V., Hans, V. S., Singh, S., Kumar, R., Pathak, S. K., Singla, M., ... & Saini, R. P. (2021). A comprehensive study on the progressive development and applications of solar air heaters. Solar Energy, 229, 112-147.